Upgrading of heavy coker naphtha by means of catalytic cracking in refinery FCC unit

Roberto Palos, Alazne Gutiérrez[*], María L. Fernández, David Trueba, Javier Bilbao, José M. Arandes

Department of Chemical Engineering, University of the Basque Country UPV/EHU, PO Box 644, 48080 Bilbao, Spain

(*) corresponding author: alazne.gutierrez@ehu.eus

ABSTRACT

The upgrading of heavy coker naphtha under conditions of the industrial fluid catalytic cracking (FCC) unit has been investigated, with the aim of obtaining light olefins and a gasoline fraction suitable to be used in the blending of motor fuels. The experiments have been conducted in a riser simulator reactor at: 500 and 550 °C; catalyst to oil mass ratio, 6 g_{cat} g_{oil}^{-1}; and, contact time, 3 to 12 s. Moreover, the effect of the properties of two commercial equilibrium catalysts on the products has been also assessed. Products have been grouped in: dry gas, liquefied petroleum gases, gasoline, light cycle oil and coke. The presence of strong acid sites in the catalyst favors the formation of light olefins, with yielding a 5 and 3.3 wt% of propylene and butenes, respectively, at 550 °C and 6 s. A higher content of zeolite (with moderate acid strength sites) and a bigger size of the mesopores of the matrix promote the formation of a commercially interesting gasoline fraction with a yield of 90 wt% under the same conditions, with a concentration of aromatics, naphthenes, *n*-paraffins, olefins and *iso*-paraffins of 25, 10, 28, 21 and 15 wt%, respectively, and a RON of 84.

1. Introduction

General trend in the extraction of petroleum has been toward heavy and low-quality oil [1,2]. Consequently, heavy oil is becoming the main feedstock of refineries all over the world and heavy oil upgrading units are playing a key role to the best utilization of resources [3]. Consequently, the establishment of thermal cracking units (i.e. visbreaker and coker units) in refineries is increasing, in order to convert the heavy fractions of products obtained in the distillation of heavy oils into lighter fractions. These fractions, in turn, will be added to the pools of fuels if their quality is good enough or upgraded in fluid catalytic cracking (FCC) or hydrotreatment units [4,5].

FCC unit aims the production of gasoline and light olefins from a variety of heavy gasoils that come from: (i) the atmospheric distillation column (atmospheric residue, AR); (ii) vacuum distillation tower (vacuum gasoil, VGO); and (iii) coker unit (coker gasoil) [6]. So, given the changes in feedstock the FCC unit is commonly submitted to and the impact that these changes have on the composition and quality of obtained products, this unit is submitted to continuous modifications and innovations [7,8].

Some of these modifications affect directly to the operating conditions the FCC unit works: higher temperature, shorter contact time, and larger catalyst to oil mass ratio (C/O) in order to further crack the heaviest feeds sufficiently [9]. Another big field of research are the improvements of FCC catalyst that must face the following challenges [10]: (i) increase diesel flexibility; (ii) maximize the production of high-value added chemicals; (iii) control flue gas emissions; and (iv) enhance the tolerance to metals poisoning. To reach these goals several studies can be found in the literature focused on tailoring the properties of the zeolite included in the catalyst [11–14], studying the effect of the binder [15–17], analyzing the catalyst deactivation by the deposition of coke and

metals [18–20] and tuning the diffusion of the reactants towards the active sites [21–23].

Nevertheless, the most significant modifications and innovations are oriented to the design and technologies applied in the FCC unit. This way, numerous technologies have been developed to modify the riser termination devices, as a poor design of them significantly increases the yields of dry gas and coke in the reactor vessel located after the riser reactor. In general, they look for increasing the efficiency and the velocity in the particle recovery to terminate the catalytic cracking reactions and shorten post-riser residence time. Among these technologies, the most important systems are [24]: fender-stripping cyclone separation system (FSC), the circulating-stripping cyclone separation system (CSC), the vortex quick separation system (VQS) and the short residence time separator system (SRTS). On the other hand, improvements can be focused on designing a new controlling system for the FCC unit as it does the multi-zone cascade-controlled (MZCC) technology [25]. MZCC technology, which is based on a multi-zone synergetic control and on the optimization of mixing the heat of catalyst and oil, improves the accessibility towards active sites in the catalyst and mass and heat transfer, leading to higher yields of liquids and lower of gases and coke.

But, the most important innovations proposed so far in FCC units are those that propose modifications in the reaction zone. So, the maximizing iso-paraffins (MIP) technology applies a sequential two-zone riser to improve gasoline and propylene yields, but also to produce an iso-paraffins rich gasoline with lower content of sulfur [26]. On the other hand, TSR (two-stage riser) technology proposes to treat fresh feedstock and cycle oil in two separate reactors to avoid competing adsorption and reaction effects to maximize light oil production [27], whereas the subsidiary riser FCC (SRFCC) process uses an

73 additional riser reactor to improve the quality of the gasoline fraction by reducing the

74 content of olefins [28,29].

75 In this context is where our research has a bearing. We have studied the upgrading of

76 heavy coker naphtha by means of catalytic cracking in a riser simulator reactor with the

77 aim of assessing the suitability of the industrial FCC unit to upgrade this secondary

78 stream (with a high content of olefins and heavy aromatics), adapting its composition to

79 the requirements of the gasoline pool of the refinery and with the production of olefins

80 as a secondary goal. In addition, two different equilibrated commercial catalysts have

81 been tested in order to investigate the effect of their properties on the products

82 distribution and composition.

83 **2. Experimental**

84 *2.1. Materials*

85 *2.1.1. Heavy coker naphtha*

86 The heavy coker naphtha (HCN), which is a thermally cracked naphtha obtained in a

87 coker unit, has been directly provided by Repsol S.A. from their facilities located in

88 Tarragona (Spain). Given the tendency of this stream to form gums when contacted

89 with oxygen, special care has been taken to store it [30]. Main physicochemical

90 properties of the HCN are collected in Table 1. Density has been estimated according to

91 ASTM D4052 Standard, whereas simulated distillation curve has been obtained

92 following the procedure described in the ASTM D2887 Standard in an Agilent 6890

93 Series GC Systems gas chromatograph equipped with an FID detector and a WCOT

94 Ultimetal semicapillary column (5 m × 0.53 mm × 0.17 μm). On the other hand, the

95 content of sulfur has been obtained by means of X-ray fluorescence spectrometry in a

96   Panalytical Axios mAX advanced apparatus according to the ASTM D4294 Standard.

97   Finally, the composition has been determined in an Agilent 7890A Series GC Systems

98   gas chromatograph equipped with an FID detector and a high-resolution Tracer

99   capillary column (60 m × 0.20 mm × 0.50 μm).

100   **Table 1.** Physicochemical properties of the heavy coker naphtha (HCN).

density at 15 °C (g cm^3)	0.7737
Simulated distillation (°C)	
IBP	67
10 wt%	109
30 wt%	134
50 wt%	152
70 wt%	166
90 wt%	183
FBP	201
Content of sulfur (wt%)	1.22
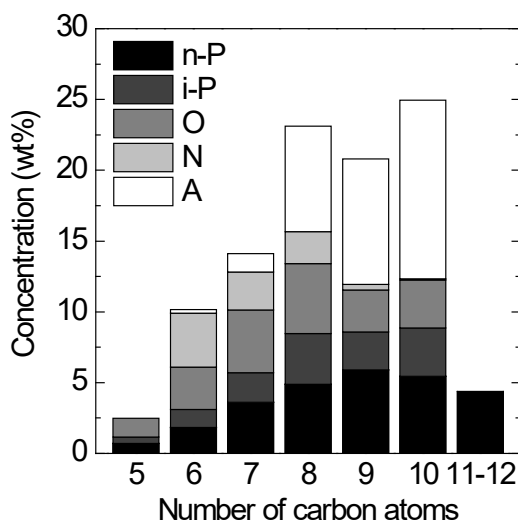
101

102   **Figure 1.** Distribution of HCN components according to their chemical nature and

103   number of carbon atoms. Key: n–P, n–paraffins; i–P, iso–paraffins; O, olefins; N,

104   naphthenes; and A, aromatics.

2.2.2. Equilibrium catalysts

106   Two different commercial equilibrium catalysts have been used for the cracking

107   experiments: ECAT-1 and ECAT-2, which have been supplied by Petronor Refinery

108   (Spain) and Petrobras (Brazil), respectively and collected from the catalyst purge stream

109   of the FCC unit. Hence, they consist on equilibrium catalysts after their circulation

110   through reaction and regeneration sections. Both catalysts have been used in the

111   corresponding refineries for the cracking of vacuum gasoil with the aim of maximizing

112   the production of gasoline fraction. The catalysts have been characterized by means of

113   several techniques and their main properties have been collected in Table 2. To

114   determine the average particle size, a number of ca. 500 particles have been analyzed

115   for each catalyst by means of scanning electron microscopy in a Hitachi S-4800

116   scanning electron microscope as described in ASTM E1382 Standard. Textural

117   properties of the catalysts have been determined by means of N_2 adsorption-desorption

118   isotherms in a Micromeritics ASAP 2010 equipment. Prior to analysis, samples have

119   been degasified at 300 °C for 8 h under vacuum in order to remove all the impurities.

120   The specific surface areas have been determined using the Brunauer-Emmett-Teller

121   (BET) surface method. The total pore volumes have been obtained from the amount of

122   N_2 adsorbed in the range of relative pressures of 0.05-0.98. The micropore volumes

123   have been estimated using the results obtained at almost insignificant relative pressures

124   (almost null). This way, obtained values are approximately a 10 % higher than those

125   obtained using the correlation of Harkins & Jura (*t*-plot method). The contents of zeolite

126   have been estimated from the N_2 adsorption isotherms following the procedure

127   described by Johnson [31]. Finally, unitary cell parameters of the USY zeolite (ASTM

128   D3942 Standard) have been determined from the X-ray diffractograms obtained in a

129   Philips X'Pert PRO powder diffractometer equipped with a PIXcel detector based on

130   the solid-state technology and a secondary monochromator with Cu-Kα radiation.

131   **Table 2.** Properties of the commercial equilibrium catalysts.

	ECAT-1	ECAT-2
Physical properties		
Average particle size (µm)	74	75
BET surface area ($m^2 g^{-1}$)	205	179
Micropore area ($m^2 g^{-1}$)	40	140
Pore volume ($cm^3 g^{-1}$)	0.25	0.17
Micropore volume ($cm^3 g^{-1}$)	0.02	0.06
Average matrix mesopore diameter (Å)	43	61
Unitary cell parameters (Å)	24.31	24.26
Chemical composition		
Al_2O_3 (wt%)	48.0	34.2
SiO_2 (wt%)	48.7	62.8
SiO_2/Al_2O_3 ratio	1.01	1.82
Rare earth oxides (wt%)	2.70	1.26
P_2O_5 (wt%)	–	0.13
TiO_2 (wt%)	–	0.39
Na (wt%)	0.17	0.50
Fe (wt%)	0.35	0.01
V (ppm)	1200	2675
Ni (ppm)	270	3995
Cu (ppm)	10	–
Catalytic properties		
USY zeolite content (%)	14	21
Total acidity ($mmol_{NH3} g^{-1}$)	0.018	0.058
Acidic strength ($kJ mol_{NH3}^{-1}$)	145	122
Brønsted/Lewis acid sites ratio	3.2	1.6

132   The chemical composition of the catalysts has been determined by means of inductively

133   coupled plasma atomic emission spectroscopy in a Horiba Jobin Yvon Activa

134   spectrometer. Prior to be introduced into the plasma, samples have been digested in

135   hydrofluoric acid to dissolve them. A relevant content of metals (Fe, Ni, V) has been

136   detected, which are accumulated in the matrix of the catalysts in the successive reaction-

137 regeneration cycles. The presence of these metals is one of the main causes of

138 irreversible deactivation of FCC catalyst, which obliges to the continuous substitution

139 of a fraction of the catalyst stream (equilibrated catalyst) by fresh catalyst. Besides,

140 these metals promote some secondary and undesired reactions, specifically the

141 hydrogen-transfer ones (Ni is the most active metal). Therefore, comparing the

142 composition of both catalysts shown in Table 2, it can be seen that ECAT-1 has higher

143 contents of Fe and Cu, whereas V and Ni are the most important metals in ECAT-2.

144 Both total acidity and acidic strength have determined by means of ammonia

145 temperature programmed desorption in a TG-DSC Setaram 111 calorimeter provided

146 with a Harvard Apparatus syringe pump and connected in-line with a Balzers Quadstar

147 422 mass spectrometer. The Brønsted/Lewis acid sites ratio has been determined by

148 Fourier transform infrared spectroscopy in a Thermo Nicolet 6700 FTIR interferometer

149 equipped with a SPECAC transmittance cell. Detailed descriptions of followed

150 experimental protocols can be found elsewhere [32,33].

151 *2.2. Cracking experiments*

152 The cracking experiments have been conducted in a CREC Riser Simulator Reactor. It

153 consists on a laboratory-scale unit, which has been patented and manufactured at the

154 University of Western Ontario (London, Canada), designed to reproduce the behavior of

155 the industrial fluid catalytic cracking (FCC) unit [34]. A detailed description of the

156 experimental procedure followed in the cracking experiments can be found in our

157 previous works [35,36]. Additionally, a schematic diagram of the unit is provided in the

158 Supplementary Material (Figure S1).

159 Investigated reaction conditions have been the following: temperature, 500 and 550 °C;

160 catalyst to oil (C/O) mass ratio, 6 g_{cat} g_{oil}^{-1}; and contact time, 3, 6, 9 and 12 s.

161 Investigated ranges for both temperature and contact time are the ones commonly used

162 in the industry to adapt the production of the FCC units to the different variations that

163 can occur in the feedstock composition, behavior of the catalyst or targeted products

164 distribution [37]. To ensure both the soundness and reproducibility of the data, each one

165 of the experiments has been repeated at least three times.

166 *2.3. Product analysis*

167 The product analysis equipment has consisted on an Agilent 7890A Series GC Systems

168 gas chromatograph equipped with an FID detector and a HP-PONA capillary column

169 (50 m × 0.20 mm × 0.50 µm). Obtained products have been grouped in several fractions

170 in agreement with the fractionation produced in refineries: dry gas (C_1-C_2), liquefied

171 petroleum gases (LPG, C_3-C_4), gasoline (C_5-C_{12}) and light cycle oil (LCO, $C_{13}-C_{20}$).

172 Given the preciseness in the identification of the reaction products, they have been also

173 classified according to their chemical nature and number of carbon atoms.

174 In addition to gas and liquid products, there has been a carbonaceous deposit formed on

175 the catalyst, which is commonly known as coke. The amount of coke formed has been

176 determined by temperature programmed oxidation in a TA Instruments TGA-Q 5000

177 thermobalance according to the procedure described by Rodríguez et al. [33].

178 *2.4. Reaction index*

179 In the catalytic cracking of heavy feeds conversion is commonly defined as the amount

180 of LCO and heavy cycle oil (HCO, C_{21+}) fractions converted into lighter products (dry

181 gas, LPG and gasoline) and condensed to coke [38,39]. Nevertheless, this definition

182 cannot be used in the cracking of the HCN as their components are within the range of

183 the gasoline fraction (Table 1). Hence, yield of each fraction *i*, which is defined as the

184 mass ratio of each particular fraction referred to the total mass fed, has been used as a

185 reaction index to determine the extent of reaction.

186 $$\text{Yield of fraction}_i \ (\text{wt}\%) = \frac{\text{mass of fraction}_i}{\text{total mass fed}} \cdot 100 \tag{1}$$

187 **3. Results**

188 *3.1. Product distribution*

189 Figure 2 shows the effect of the contact time on the product distribution obtained in the

190 cracking of heavy coker naphtha (HCN) with ECAT-1 at 500 and 550 °C (Figure 2a and

191 b, respectively). These results expose the influence of the contact time, which is

192 equivalent to the longitudinal position along the riser reactor of the industrial unit, in

193 obtained results. During the first 9 s of contact, the cracking reactions evolve leading to

194 lower yields of gasoline and higher of dry gas and LPG fractions. From this time of

195 contact on, obtained yields reach almost constant values. However, it can be seen that at

196 500 °C (Figure 2a) neither the LCO fraction nor the coke one follow this pattern. LCO

197 fraction goes through a maximum for a contact time of 7-8 s and reaches its minimum

198 value at 12 s, whereas the deposition of coke is maximized at short times (3 s at 500 °C

199 and 6 s at 550 °C).

200 Focusing on the effect of the temperature, it can be seen that an increase of 50 °C in the

201 reaction temperature entails an increase of the over-cracking reactions that promote the

202 formation of dry gas and LPG fractions in detriment of the gasoline one. On the other

203 hand, the yields of LCO fraction and coke are practically not influenced by the increase

204 of temperature. Similar trends have been observed in the cracking of VGO both in a

205 riser simulator reactor [40] and in a pilot-scale FCC apparatus [41]. Indeed, in the latter

206 case, the yields of dry gas and LPG fractions obtained at 500 °C and C/O of 6 $g_{cat} \ g_{oil}^{-1}$

207 are similar to the ones obtained in this work in the cracking of HCN. However, in the

208 cracking of the VGO, the yield of gasoline fraction is strongly affected by over-cracking

209 reactions and goes through an intermediate maximum.
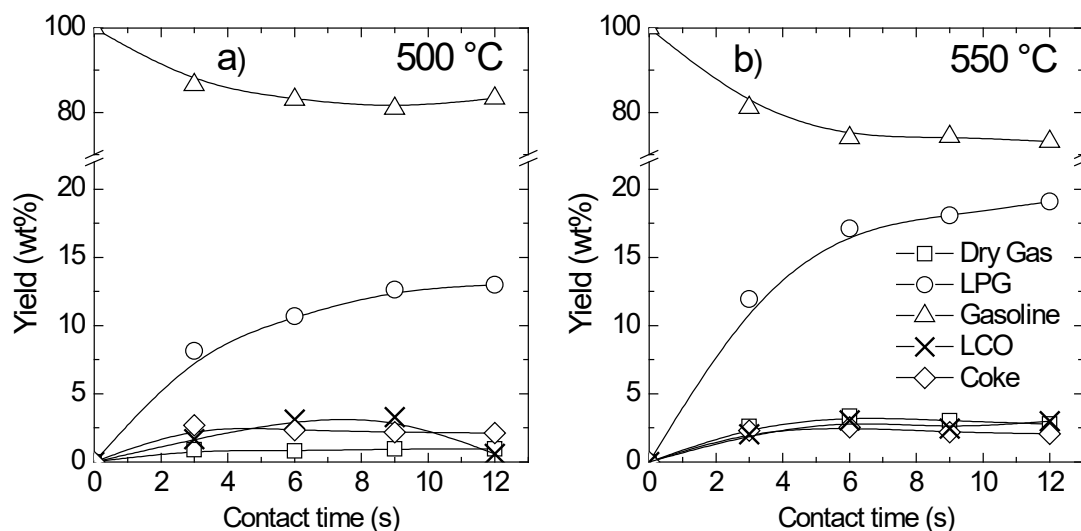
210

211 **Figure 2.** Evolution with contact time of the yields of the different product fractions

212 obtained at 500 °C (a) and 550 °C (b) with catalyst ECAT-1.

213 In order to properly understand the effect of both temperature and contact time on the

214 yields of the different fractions, the mechanism of catalytic cracking reaction must be

215 taken into account. The reaction network involves four main catalytic pathways [10,42]:

216 (i) carbonium ion formation by means of proton transfer from zeolite Brønsted sites to

217 alkanes; (ii) carbenium ion formation by proton transfer from zeolites to alkenes; (iii)

218 hydride transfer from alkanes to zeolites to forming carbenium ions; and (iv) β-scission

219 reaction of a carbenium ion forming a primary carbenium ion and an alkene. These

220 catalytic steps, which are promoted at high temperatures, are inhibited by the catalyst

221 deactivation and have to compete with thermal cracking mechanisms. The latter group

222 of reactions occur through homolytic cleavage of C–C bonds that lead to the formation

223 of free radicals that undergo subsequent β-scission reactions [43]. Hence, high

224 temperature will promote the formation of ethylene and other methyl- and ethyl-groups

225 free radicals that combine with other hydrogen-free radicals to stabilize in the form of

226 methane, ethane and hydrogen [44]. In addition, a continue formation of dry gas can be

227 assumed because of the interaction of H^+ ions with the pentacoordinated carbonium ions

228 obtained in the monomolecular cracking of alkanes [45].

229 The formation of coke principally occurs at short contact times (< 3 s), which is a fact

230 commonly observed in FCC units in the catalytic cracking of heavy feeds [46,47]. The

231 formation of coke can follow several pathways [20,48], being the most important those

232 that lead to the formation of: (i) additive coke and (ii) catalytic coke. This way, additive

233 coke has a thermal origin and is formed by the deposition of poly-aromatic compounds

234 that lead to the blockage of the micropores of the catalyst. On the other hand, catalytic

235 coke is the product obtained in bimolecular hydrogen-transfer reactions via aromatics

236 intermediates. The extent and evolution degree of the reactions that lead to the

237 formation of this type of coke strongly depend on the properties of the catalyst,

238 composition of the feedstock and operating conditions. In addition, additive and

239 catalytic cokes are also known as external and internal cokes, respectively, depending

240 on the coke location on the zeolite. Considering the boiling range of the HCN (Table 1),

241 it can be assumed that the type of coke that will be preferentially formed is the catalytic

242 one as the molecules will reach and access the channels of the zeolite.

3.2. Composition of the gas fraction

244 Figure 3 collects the effect of the contact time on the concentration of the different

245 gaseous compounds (C_1–C_3 on Figure 3a-b and C_4 on Figure 3c-d) for the studied

246 temperatures (500 and 550 °C). It should be highlighted that gases are formed at short

247 contact times and that their concentration is barely modified with the course of time. On

248 the other hand, an increase of the temperature from 500 to 550 °C promotes the

249 formation of C_1–C_3 gases in detriment of the C_4 ones, meaning that cracking reactions

250 are selectively favored at high temperatures with respect to dehydrogenation and

251 isomerization ones [49].
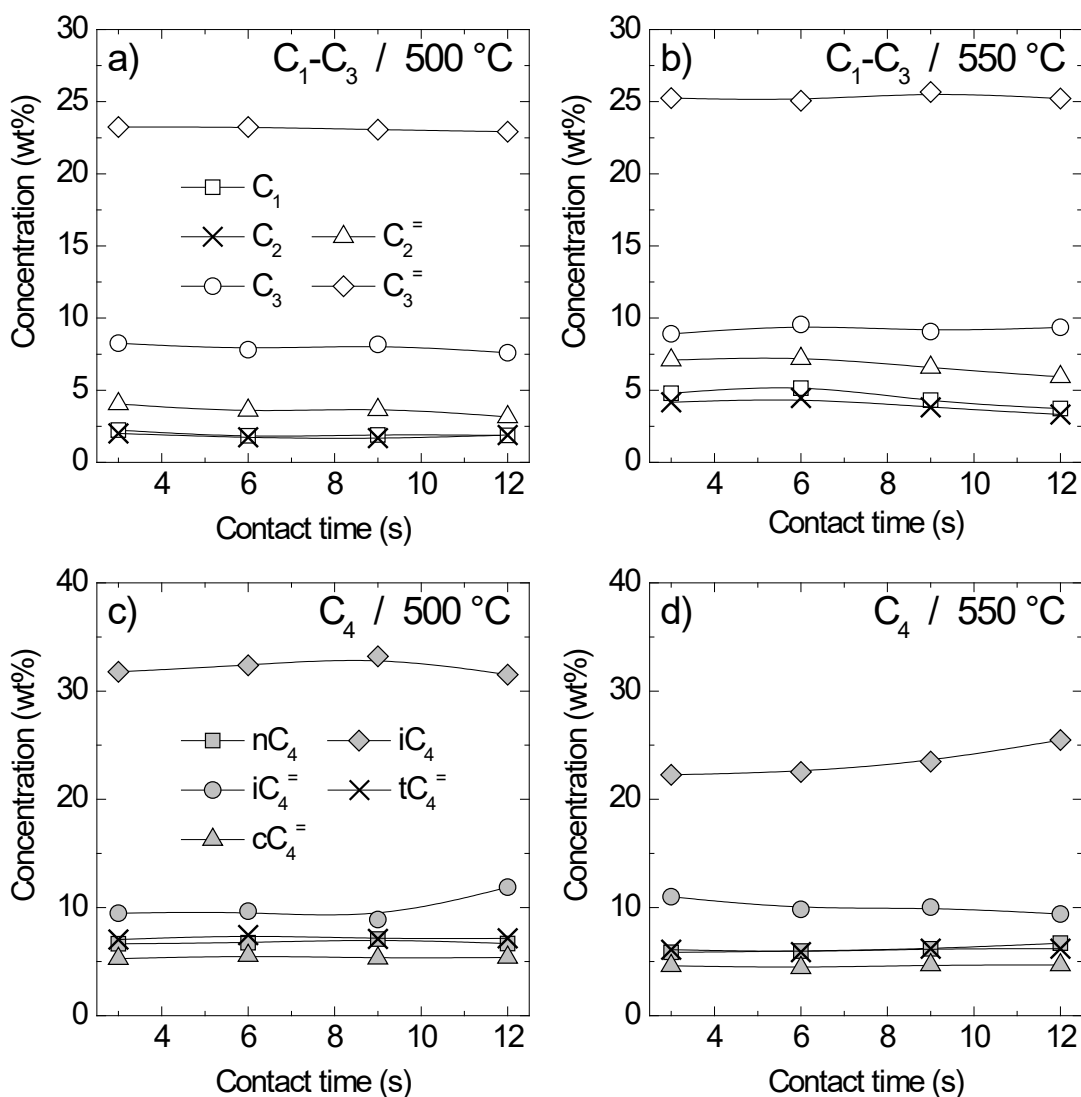
252

253 **Figure 3.** Evolution with contact time of the composition of the gas fraction obtained

254 with catalyst ECAT-1 in the catalytic cracking of HCN. Graphs (a) and (b) correspond

255 to C_1–C_3 compounds at 500 and 550 °C, respectively. Graphs (c) and (d) correspond to

256 the different C_4 isomers.

257   Attending to the results collected in Figure 3, most abundant products in the gaseous

258   fraction are: iso-butane (iC_4), propylene ($C_3^=$), iso-butene ($iC_4^=$) and propane (C_3), with

259   the yields in the ranges of 22.3-33.2, 22.9-25.7, 9.4-11.9 and 7.5-9.6 wt%, respectively.

260   Konno et al. [50] have obtained similar distributions of the gaseous products in the

261   catalytic cracking of synthetic naphthas. Nevertheless, the concentration of ethylene and

262   propylene, which are the most attractive olefins to be marketed, can be increased by

263   using zeolite-based catalysts modified with HZSM-5 zeolite [51] or by tailoring the

264   porous structure of the catalyst decreasing the diffusion resistances [52].

265   In order to have a brief idea of the mechanisms that govern the cracking of the HCN, the

266   cracking mechanism ratio (CMR) has been determined at both 500 and 550 °C. This

267   parameter is a measure of protolytic cracking to β-scission reactions as C_1-C_2 products

268   reflect protolytic cracking, while iC_4 reflects the formation of products through β-

269   scission of ramified hydrocarbons [53]. CMR values are in the range of 0.26-0.22 and

270   0.72-0.51 for the temperature of 500 and 550 °C, meaning that high temperatures

271   promote the protolytic cracking reactions, whereas long contact times the β-scission

272   ones.

273   Olefinicity is a result of a competition between cracking and hydrogen-transfer

274   reactions, which are producing and consuming olefins, respectively. This parameter

275   ($C_x^=/C_{x\text{-Total}}$ mass ratio) is commonly used to determine the quality of the LPG fraction.

276   This way, the olefinicity of the C_3 compounds remains almost constant with temperature

277   and contact time in values of ca. 0.74. On the other hand, the olefinicity of C_4

278   compounds increases with temperature from 0.39-0.35 at 500 °C to 0.44-0.39 at 550 °C.

279   This trend is a consequence of: (i) the boosting of the cracking reactions at higher

280   temperatures because of their higher activation energy; and (ii) the inhibition of the

281   hydrogen-transfer reactions because they are thermodynamically disfavored at high

282   temperatures given their exothermic nature. On the contrary, longer contact times

283   promote hydrogen-transfer reactions causing a decrease of the olefinicity of the C_4

284   compounds, as observed by Passamonti et al. [54] in the catalytic cracking of VGO.

285   These authors relate the notorious reduction of the concentration of iso-butane when

286   increasing cracking temperature (evident effect in Figure 3c and 3d) to formation

287   mechanisms of this molecule. This way, it can obtained trough hydrogen-transfer of a

288   butene, but also in the cracking of components within the gasoline fraction. Furthermore

289   the increase of the concentration of C_3 compounds with temperature, while C_4 species

290   are reduced, can be related to the selective cracking of the olefins of the gasoline

291   fraction, with a preferential formation of ethylene and propylene [40].

292   *3.3. Composition of the gasoline fraction*

293   The composition of the gasoline fraction has been analyzed by chromatographic means

294   and the effect of both temperature and contact time has been depicted in Figure 4. It can

295   be seen that the concentration of iso-paraffins (i-P) increases with contact time, while

296   those of olefins (O) and naphthenes (N) decrease. Besides, there are no big differences

297   among the results obtained at 500 (Figure 4a) and at 550 °C (Figure 4b) for these

298   families of compounds. On the other hand, linear paraffins (n-P) and aromatics (A)

299   show opposite trends as the former shows an increasing trend at 500 °C and decreasing

300   at 550 °C and the latter a decreasing trend at 500 °C and decreasing at 550 °C.

301   Comparing the composition of produced gasoline fractions with that of the HCN several

302   changes are observed. For both temperatures of 500 and of 550 °C the concentration of

303   iso-paraffins and of olefins are mainly modified. This way, the concentration of iso-

304   paraffins increases at least a 7 wt% at 500 °C and a 5 wt% at 550 °C, whereas that of

305   olefins decreases at least a 6 wt% at 500 °C and a 3 wt% at 550 °C. With regard to the

306 remaining families of compounds, bigger differences have been observed at 500 °C with

307 an increasing concentration of n-paraffins and decreasing of naphthenes and aromatics.

308 At 550 °C, in turn, the concentrations of n-paraffins and aromatics remain in values

309 similar to those of the feed and the concentration of naphthenes decreases. The different

310 trend in the concentration of aromatics can be assigned to: (i) an increase of the

311 condensation reactions at 550 °C that lead to obtain bigger amounts of aromatics and

312 heavier molecules; and (ii) promotion of the cracking reactions of the lateral chains of

313 the aromatics compounds at 500 °C that convert them in lighter molecules.
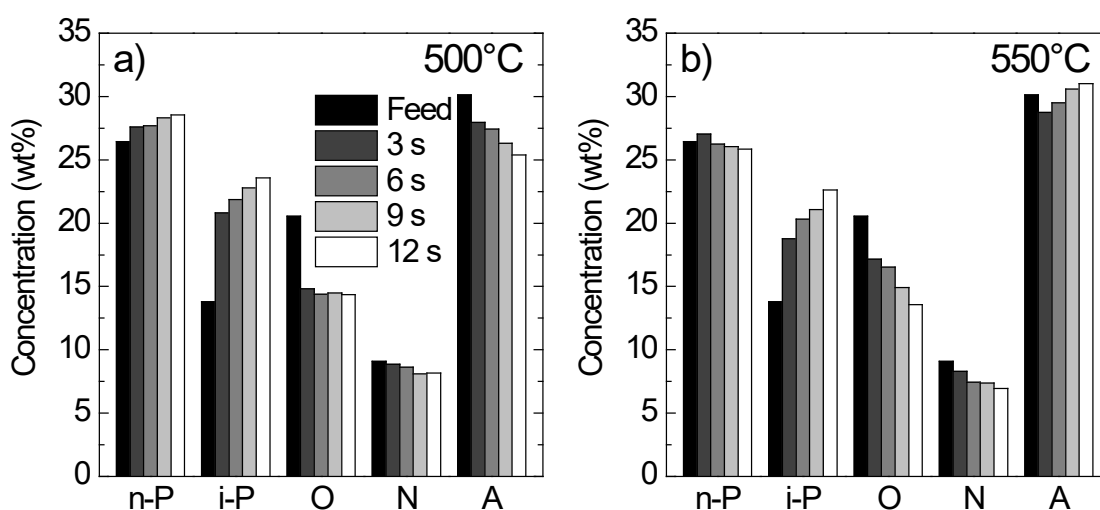
314

315 **Figure 4.** Effect of the contact time on the concentration of families of compounds of

316 the gasoline fraction obtained in the catalytic cracking of HCN at 500 (a), and 550 °C

317 (b) with catalyst ECAT-1. Key: n–P, n–paraffins; i–P, iso–paraffins; O, olefins; N,

318 naphthenes; and A, aromatics.

319 The evolution of the concentration of aromatics with contact time relies on the

320 refractoriness of the C–C bonds of the aromatic ring and its formation by means of

321 cyclization of olefins and dehydrogenation of naphthenes [55,56]. Indeed, a proper

322 analysis of the effect of the operating conditions on these reactions is a complex task

323   given the different nature of the reactions. This way, the formation of aromatics by

324   Diels-Alder cyclization of olefins is boosted at high temperatures and long contact

325   times. However, the formation of aromatics by means of hydrogen-transfer reactions via

326   naphthenes intermediates are inhibited at high temperatures but boosted at long contact

327   times [57].

328   For a more detailed analysis of the effect of the temperature on the composition of the

329   gasoline fraction for the different families of compounds grouped according to their

330   number of carbon atoms has been listed in Table S1 in the Supplementary Material.

331   Note that results have been for a contact time of 6 s, as they show an intermediate

332   behavior of the catalytic cracking of the HCN. Attending to linear paraffins in the first

333   place, their distribution in the HCN shows the highest concentration in the range of C_8–

334   C_{10}, which does not suffer high variations (ca. 1 wt%) at none of the tested temperatures

335   given the low reactivity of this family of compounds. In spite of their global low

336   reactivity, high-molecular weight paraffins (C_{10}–C_{11}) are more affected by cracking

337   reactions leading to the formation of lighter n-paraffins (C_5–C_6). This redistribution

338   within this family of compounds is far more evident at 550 than at 500 °C, as cracking

339   reactions are boosted at high temperatures.

340   The high reactivity of the iso-paraffins and of the olefins is clearly reflected in the

341   results obtained at both temperatures. Regarding iso-paraffins, their high concentration

342   in the HCN is in the range of C_8–C_{10}, which is rapidly cracked to lighter fractions in the

343   range of C_5–C_7. The effect of the temperature is quite evident for these compounds as at

344   500 °C just the C_9 and C_{10} molecules react, while at 550 °C even the C_8 ones are

345   substantially reduced. A similar behavior has been obtained for the olefins. The C_7–C_8

346   olefins the predominant ones in the HCN, but they are substantially reduced together

347   with the C_9–C_{10} ones. In addition, temperature has a strong effect as an increase from

348   500 to 550 °C further converts the C_7–C_{11} olefins to form lighter ones within the

349   gasoline range (C_5–C_6) and in the LPG fraction (C_3–C_4).

350   Finally, lighter aromatic compounds (C_6–C_9) have been obtained in the gasoline fraction

351   at both 500 and 550 °C comparing with the composition of the HCN. This reduction is

352   more marked at 550 than at 500 °C, meaning that aromatic rings are hardly cracked, but

353   do they are their lateral chains.

354   In order to define the properties of the gasoline fraction, several indices are commonly

355   computed: research octane number (RON) [58], olefinicity ($C_x^=$/$C_{x\text{-Total}}$ mass ratio), iso-

356   paraffinicity (i-C_x/n-C_x mass ratio) and iso-olefinicity (i-$C_x^=$/n-$C_x^=$ mass ratio). Obtained

357   values have been collected in Table 3. RON is the most meaningful one and close

358   values to that of the HCN (84.2) have been obtained, slightly lower at 500 °C (82.9) and

359   practically a similar value at 550 °C (84.3). The content of olefins increases with

360   reaction temperature both for C_5 and for C_6 molecules, meaning that the cracking of

361   paraffins that lead to the formation of olefins is boosted at high temperatures. The

362   branching of paraffins and olefins within the gasoline fraction decreases with

363   temperature because of the aforementioned higher reactivity of the ramified chains.

Table 3. Effect of the temperature and of the catalyst on the quality indices of the gasoline fraction obtained for a contact time of 6 s.

| Quality index	ECAT-1		ECAT-2
	500 °C	550 °C	550 °C
olefinicity			
$C_5^=/C_{5\text{-Total}}$	0.27	0.34	0.46
$C_6^=/C_{6\text{-Total}}$	0.24	0.25	0.41
iso-paraffinicity			
$i\text{-}C_5/n\text{-}C_5$	5.04	4.26	2.62
$i\text{-}C_6/n\text{-}C_6$	2.03	1.70	0.72
iso-olefinicity			
$i\text{-}C_5^=/n\text{-}C_5^=$	1.49	1.48	1.22
$i\text{-}C_6^=/n\text{-}C_6^=$	1.35	1.11	0.98
RON	82.9	84.3	83.4

3.4. Effect of the properties of the catalyst

The catalytic cracking of HCN has been afforded with catalyst ECAT-2 to assess the effect of the properties of the catalyst (Table 2) on the products distribution and on their composition. Thus, the effect of the contact time on the yield of the fractions obtained at 550 °C with ECAT-2 has been depicted in Figure 5 together with those previously reported in Figure 2b to facilitate the comparison of obtained results. Note that ECAT-2 has been only tested at 550 °C because at this temperature the effect of the acidic and chemical properties of the catalyst are maximized and a clearer and more fruitful comparison can be done. Comparing the results obtained with both catalysts, it can be seen that the yield of gasoline fraction (Figure 5a) decreases more slowly with ECAT-2 than with ECAT-1. Furthermore, lower yields of LPG and LCO fractions have been

377   obtained with ECAT-2 (Figures 5a and 5b, respectively), while the yields of dry gas and

378   coke are superior to those of ECAT-1 (Figure 5b). The rapid deposition and high

379   content of coke of ECAT-2 contributes to an attenuation of the catalytic activity and its,

380   subsequent, rapid deactivation. This interpretation is consequent with the low yield of

381   LPG obtained, which is the fraction directly obtained in the cracking of the gasoline one

382   [59]. Likewise, is in concordance with the higher yield of dry gas, whose formation is

383   related to the thermal cracking that is promotes by the catalyst deactivation. The

384   different performance of the catalyst is related to their physicochemical properties

385   (Table 2). Total acidity is notoriously greater in ECAT-2 (0.058 $mmol_{NH3}$ g^{-1}) than in

386   ECAT-1 (0.018 $mmol_{NH3}$ g^{-1}). However, the average acid strength is greater for ECAT-

387   1 than for ECAT-2 (145 and 122 kJ mol_{NH3}^{-1}, respectively). This way, the former

388   catalyst has a lower density of superficial acid sites, but these sites are strongly acid.

389   The different Brønsted/Lewis acid sites ratio obtained for both catalysts (3.2 for ECAT-

390   1 and 1.6 for ECAT-2) is in concordance with the different strength of the acid sites, as

391   it is accepted that Brønsted-type acid sites are of greater acid strength.

392   The higher content of coke of ECAT-2 (Figure 5b) can be attributed to its higher total

393   acidity and content of zeolite (Table 2) that boost the condensation reactions of the

394   aromatics [48]. Furthermore, the considerable higher content of Ni in ECAT-2 can also

395   promote the formation of coke as it even promotes in a higher extent the condensation

396   reactions that lead to the formation of coke [60]. Moreover, ECAT-1 has a higher

397   content or rare earth oxides that confer a higher hydrothermal stability to the zeolite and

398   contributes to avoid undesired reactions, such as the condensation ones [61]. Porous

399   structure of the catalyst can also be crucial in the formation of coke. This way, a

400   structure with a higher content of mesopores, like that of ECAT-2 (Table 2), could hold

401   up the deactivation of the catalyst by blocking of the channels of the zeolite, but it will

402   at the same time ease the condensation of poly-aromatic structures that act as coke

403   precursors. Attending to the content of coke (Figure 5b), it can be assumed that the

404   latter case is the predominant one with ECAT-2.
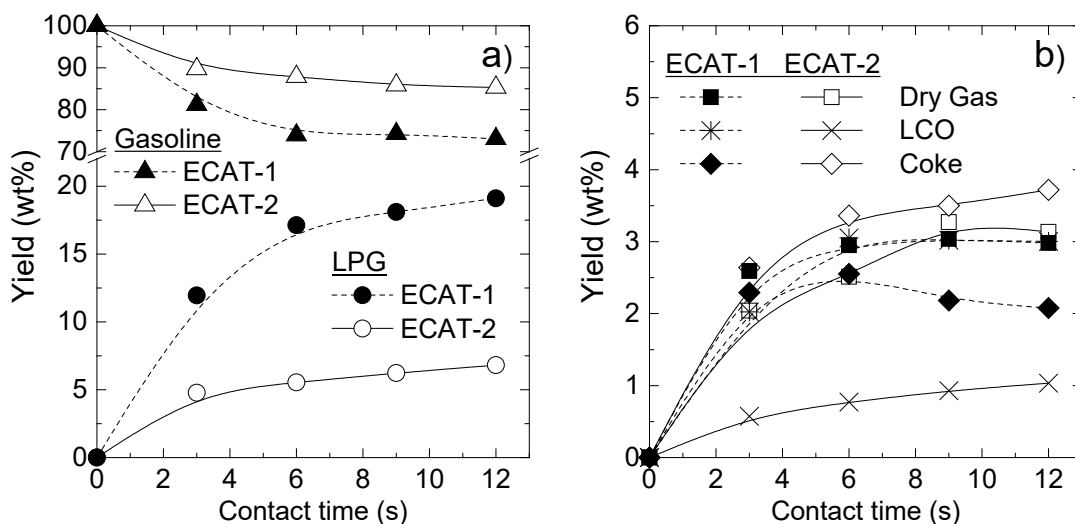

405

406   **Figure 5.** Evolution with contact time of the yields of the gasoline and LPG fractions

407   (a), and dry gas, LCO and coke fractions (b) at 550 °C with both catalysts.

408   For a proper comparison of the LPG fraction obtained with both catalysts (Figure 5a),

409   the olefinicity indices of the LPG fraction obtained with ECAT-2 at 550 °C for a contact

410   time of 6 s have been also determined. While for ECAT-1 obtained values have been of

411   0.74 and 0.45 for C_3 and C_4 molecules, respectively, the values obtained with ECAT-2

412   have been of 0.50 and 0.68, respectively. Thus, the LGP fraction obtained with ECAT-2

413   has a lower content of olefins because of its rapid deactivation and loss of cracking

414   capacity of the olefins within the gasoline fraction to lighter ones.

415   The composition of the gasoline fraction obtained with both catalysts at a temperature

416   of 550 °C for a contact time of 6 s has been compared in Figure 6. Please note that the

417   data corresponding to the feed and to ECAT-1 have been reproduced from Figure 4b for

418   the sake of the comparison with the results obtained with ECAT-2. As it can be seen in

419   Figure 6, the catalyst used clearly conditions the composition of the gasoline fraction

420   obtained. Hence, in the composition obtained with ECAT-2 stands out the reduction of

421   the content of aromatic compounds and the increase of the concentration of n-paraffins,

422   olefins and naphthenes. Given the refractoriness of the aromatic compounds, the lower

423   content of aromatics is mainly attributed to the branching of lateral chains instead of to

424   ring-opening reactions.

425   Based on the results obtained with ECAT-1 and ECAT-2 (Figure 4b and Figure 6,

426   respectively) and from the expectation of upgrading the HCN in FCC units, ECAT-1

427   appears as a good option in order to obtain an olefin-rich LPG fraction. On the other

428   hand, ECAT-2 is appropriate to produce a gasoline fraction suitable to be incorporated

429   in the blending of the commercial pool of gasoline given its moderate content of

430   aromatics.
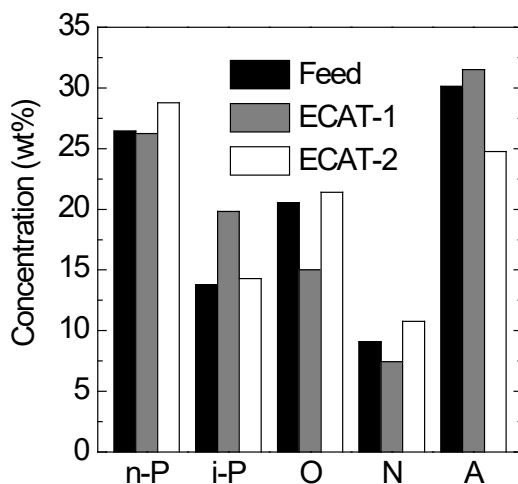
431

432   **Figure 6.** Comparison of the composition of the gasoline fraction obtained with the

433   different catalysts. Conditions: temperature, 550 °C; and contact time, 6 s. Key: n–P, n–

434   paraffins; i–P, iso–paraffins; O, olefins; N, naphthenes; and A, aromatics.

435 Additionally, the indices that determine the properties of the gasoline fraction have been

436 also determined for the gasoline obtained with ECAT-2. Obtained values for the

437 olefinicity, iso-paraffinicity, iso-olefinicity and RON have been tabulated in Table 3. As

438 aforementioned, the olefinicity of gasoline fraction obtained with ECAT-2 is higher

439 than that obtained with ECAT-1, meaning that hydrogen-transfer reactions are more

440 inhibited with ECAT-2 than with ECAT-1. This inhibition is a consequence of the rapid

441 formation of coke that occurs with ECAT-2, which partially deactivates the catalyst

442 hindering the cracking of these rather heavy olefins to lighter ones that will be part of

443 dry gas and LPG fractions. The attenuation of the hydrogen-transfer capacity of the

444 catalyst caused by the fast coke deposition has been already observed by Passamonti et

445 al. [62] when comparing catalysts with different hydrogen-transfer capacity. On the

446 other hand, gasoline fraction obtained with ECAT-1 is more ramified, i.e. higher values

447 of iso-paraffinicity, because of the higher isomerization capacity of this catalyst.

448 Finally, the RON obtained with both catalyst are quite similar in spite of the different

449 composition of the gasoline fraction obtained with each of them.

450 **4. Conclusions**

451 Obtained results expose the interest of upgrading heavy coker naphtha by means of

452 catalytic cracking in the FCC unit. The properties of the catalyst used strongly affect the

453 distribution and composition of the fractions obtained. This way, a catalyst with the

454 properties of ECAT-1 (high acid strength and Brønsted/Lewis ratio) should be

455 preferably used when LPG fraction and light olefins (ethylene, propylene and butenes)

456 are targeted. Olefinicity indices of the fraction C_3–C_4 increases with temperature as

457 cracking reactions are preferentially boosted instead of hydrogen-transfer ones,

458 obtaining at 550 °C and a contact time of 6 s a yield of propylene of 5 wt% and of

459 butenes of 3.3 wt%. For a gasoline fraction suitable to be used in the blending of

460   automotive fuels, a catalyst with a high density of acid sites with moderate strength

461   (such as ECAT-2) offers better results.

462   The composition of the gasoline fraction (C_5-C_{12}) evolves with contact time, so at long

463   contact times the concentration of olefins and naphthenes is reduces, while that of iso-

464   paraffins increases. These results rely on the promotion of the cracking reactions and on

465   the high reactivity of the olefins and naphthenes, especially those of bigger molecular

466   weight. Consequently, at longer contact times the concentration of C_{9+} olefins is

467   reduced and that of C_5-C_8 increases. The concentration of aromatics remains almost

468   constant in the products, but lighter molecules (in the C_6-C_8 range) form it because of

469   the branching of the lateral chains of C_{9+} aromatics, reducing the average molecular

470   weight of the family of aromatics. On the contrary, temperature has not a marked effect

471   on the composition of the gasoline fraction obtained. It has been obtained a yield of

472   gasoline of 90 wt% with ECAT-2 at 550 °C and for a contact time of 6 s, whose

473   concentration of aromatics, naphthenes, n-paraffins, olefins and *iso*-paraffins is of 25,

474   10, 28, 21 and 15 wt%, respectively, and its RON is of 84.

475   As aforementioned, the yields obtained for the dry gas, LPG and coke fractions in the

476   cracking of HCN are similar to those reported in the literature for the cracking of VGO.

477   Based on this and on the appropriate composition of the gasoline fraction obtained, it

478   will be interesting to study the co-feeding of heavy coker naphtha together with VGO to

479   the FCC unit.

References

[1]   R. Dittmeyer, M. Klumpp, P. Kant, G. Ozin, Crowd oil not crude oil, Nat. Commun. 10 (2019) 1–8. doi:10.1038/s41467-019-09685-x.

[2]   Y. Liu, S. Lu, X. Yan, S. Gao, X. Cui, Z. Cui, Life cycle assessment of petroleum refining process: A case study in China, J. Clean. Prod. 256 (2020) 120422. doi:10.1016/j.jclepro.2020.120422.

[3]   H. Ritchie, M. Roser, Fossil fuels, (2018). https://ourworldindata.org/fossil-fuels (accessed March 13, 2020).

[4]   A. Corma, E. Corresa, Y. Mathieu, L. Sauvanaud, S. Al-Bogami, M.S. Al-Ghrami, A. Bourane, Crude oil to chemicals: light olefins from crude oil, Catal. Sci. Technol. 7 (2017) 12–46. doi:10.1039/C6CY01886F.

[5]   M.S. Rana, V. Sámano, J. Ancheyta, J.A.I. Diaz, A review of recent advances on process technologies for upgrading of heavy oils and residua, Fuel. 86 (2007) 1216–1231. doi:10.1016/j.fuel.2006.08.004.

507 [6] A. Ishihara, Preparation and reactivity of hierarchical catalysts in catalytic
508 cracking, Fuel Process. Technol. 194 (2019) 106116.
509 doi:10.1016/j.fuproc.2019.05.039.

510 [7] V. Chuzlov, G. Nazarova, E. Ivanchina, E. Ivashkina, I. Dolganova, A. Solopova,
511 Increasing the economic efficiency of gasoline production: Reducing the quality
512 giveaway and simulation of catalytic cracking and compounding, Fuel Process.
513 Technol. 196 (2019) 106139. doi:10.1016/j.fuproc.2019.106139.

514 [8] H. Luan, J. Lin, G. Xiu, F. Ju, H. Ling, Study on compositions of FCC flue gas
515 and pollutant precursors from FCC catalysts, Chemosphere. 245 (2020) 125528.
516 doi:10.1016/j.chemosphere.2019.125528.

517 [9] J. Gao, C. Xu, C. Lu, C. Yang, G. Wang, X. Lan, Y. Zhang, Novel fluid catalytic
518 cracking processes, in: Y. Cheng, F. Wei, Y. Jin (Eds.), Multiph. React. Eng.
519 Clean Low-Carbon Energy Appl., John Wiley & Sons, Inc., Hoboken, NJ, USA,
520 2017: pp. 1–48. doi:10.1002/9781119251101.

521 [10] E.T.C. Vogt, B.M. Weckhuysen, Fluid catalytic cracking: recent developments
522 on the grand old lady of zeolite catalysis, Chem. Soc. Rev. 44 (2015) 7342–7370.
523 doi:10.1039/c5cs00376h.

524 [11] A.I. Hussain, A. Palani, A.M. Aitani, J. Čejka, M. Shamzhy, M. Kubů, S.S. Al-
525 Khattaf, Catalytic cracking of vacuum gasoil over -SVR, ITH, and MFI zeolites
526 as FCC catalyst additives, Fuel Process. Technol. 161 (2017) 23–32.
527 doi:10.1016/j.fuproc.2017.01.050.

528 [12] N. Masoumifard, R. Guillet-Nicolas, F. Kleitz, Synthesis of engineered zeolitic
529 materials: From classical zeolites to hierarchical core–shell materials, Adv.
530 Mater. 30 (2018). doi:10.1002/adma.201704439.

531 [13] U.J. Etim, P. Bai, Y. Wang, F. Subhan, Y. Liu, Z. Yan, Mechanistic insights into

532 structural and surface variations in Y-type zeolites upon interaction with binders,

533 Appl. Catal. A Gen. 571 (2019) 137–149. doi:10.1016/j.apcata.2018.12.013.

534 [14] Y.S. Zhang, X. Lu, R.E. Owen, G. Manos, R. Xu, F.R. Wang, W.C. Maskell,

535 P.R. Shearing, D.J.L. Brett, Fine structural changes of fluid catalytic catalysts

536 and characterization of coke formed resulting from heavy oil devolatilization,

537 Appl. Catal. B Environ. 263 (2020) 118329. doi:10.1016/j.apcatb.2019.118329.

538 [15] B. Wang, N. Li, Q. Zhang, C. Li, C. Yang, H. Shan, Studies on the preliminary

539 cracking: The reasons why matrix catalytic function is indispensable for the

540 catalytic cracking of feed with large molecular size, J. Energy Chem. 25 (2016)

541 641–653. doi:10.1016/j.jechem.2016.02.014.

542 [16] S. Tarighi, N. Modanlou Juibari, M. Binaeizadeh, Different binders in FCC

543 catalyst preparation: Impact on catalytic performance in VGO cracking, Res.

544 Chem. Intermed. 45 (2019) 1737–1752. doi:10.1007/s11164-018-3700-x.

545 [17] L. Lakiss, J.-P. Gilson, V. Valtchev, S. Mintova, A. Vicente, A. Vimont, R.

546 Bedard, S. Abdo, J. Bricker, Zeolites in a good shape: Catalyst forming by

547 extrusion modifies their performances, Microporous Mesoporous Mater. 299

548 (2020) 110114. doi:10.1016/j.micromeso.2020.110114.

549 [18] E. Rodríguez, G. Elordi, J. Valecillos, S. Izaddoust, J. Bilbao, J.M. Arandes, P.

550 Castaño, Coke deposition and product distribution in the co-cracking of waste

551 polyolefin derived streams and vacuum gas oil under FCC unit conditions, Fuel

552 Process. Technol. 192 (2019) 130–139. doi:10.1016/j.fuproc.2019.04.012.

553 [19] J. Fals, J.R. García, M. Falco, U. Sedran, Coke from SARA fractions in VGO.

554 Impact on Y zeolite acidity and physical properties, Fuel. 225 (2018) 26–34.

555   doi:10.1016/j.fuel.2018.02.180.

556   [20]   G. Nazarova, E. Ivashkina, E. Ivanchina, A. Oreshina, I. Dolganova, M.

557   Pasyukova, Modeling of the catalytic cracking: Catalyst deactivation by coke and

558   heavy   metals,   Fuel   Process.   Technol.   200   (2020)   106318.

559   doi:10.1016/j.fuproc.2019.106318.

560   [21]   X. Dong, S. Shaikh, J.R. Vittenet, J. Wang, Z. Liu, K.D. Bhatte, O. Ali, W. Xu, I.

561   Osorio, Y. Saih, J.-M. Basset, S.A. Ali, Y. Han, Fine tuning the diffusion length

562   in hierarchical ZSM-5 to maximize the yield of propylene in catalytic cracking of

563   hydrocarbons,   ACS   Sustainable   Chem.   Eng.   6   (2018)   15832–15840.

564   doi:10.1021/acssuschemeng.8b04441.

565   [22]   A. Zhokh, P. Strizhak, Crossover between Fickian and non-Fickian diffusion in a

566   system with hierarchy, Microporous Mesoporous Mater. 282 (2019) 22–28.

567   doi:10.1016/j.micromeso.2019.03.016.

568   [23]   P. Peng, D. Stosic, X.M. Liu, Z.F. Yan, S. Mintova, Strategy towards enhanced

569   performance of zeolite catalysts: Raising effective diffusion coefficient versus

570   reducing   diffusion   length,   Chem.   Eng.   J.   385   (2020)   123800.

571   doi:10.1016/j.cej.2019.123800.

572   [24]   Z. Li, C.X. Lu, FCC riser quick separation system: a review, Pet. Sci. 13 (2016)

573   776–781. doi:10.1007/s12182-016-0119-0.

574   [25]   J. Gao, Y. Mao, C. Xu, A coking inhibiting method for RFCC disengager, China

575   Patent, CN200310121301.1, 2003.

576   [26]   Y. Xu, S. Cui, A novel fluid catalytic cracking process for maximizing iso-

577   paraffins: from fundamentals to commercialization, Front. Chem. Sci. Eng. 12

578   (2018) 9–23. doi:10.1007/s11705-017-1696-1.

579 [27] J. Zhang, H. Shan, X. Chen, C. Li, C. Yang, Multifunctional two-stage riser fluid

580   catalytic cracking process, Appl. Petrochemical Res. 4 (2014) 395–400.

581   doi:10.1007/s13203-014-0079-5.

582 [28] G. Wang, G. Yang, C. Xu, J. Gao, A novel conceptional process for residue

583   catalytic cracking and gasoline reformation dual-reactions mutual control, Appl.

584   Catal. A Gen. 341 (2008) 98–105. doi:10.1016/j.apcata.2008.02.031.

585 [29] Y. Wen, G. Wang, C. Xu, J. Gao, Study on in situ sulfur removal from gasoline

586   in fluid catalytic cracking process, Energy Fuels. 26 (2012) 3201–3211.

587   doi:10.1021/ef300499j.

588 [30] F. Li, F.X. Zhang, H. Jiang, S.L. Zhao, P. Li, Effect of active acidic compounds

589   on storage stability of coker naphtha, Chem. Pap. 70 (2015) 180–187.

590   doi:10.1515/chempap-2015-0180.

591 [31] M.F.L. Johnson, Estimation of the zeolite content of a catalyst from nitrogen

592   adsorption isotherms, J. Catal. 52 (1978) 425–431. doi:10.1016/0021-

593   9517(78)90346-9.

594 [32] A.S. Al-Dughaither, H. de Lasa, HZSM-5 zeolites with different SiO_2/Al_2O_3

595   ratios. Characterization and NH_3 desorption kinetics, Ind. Eng. Chem. Res. 53

596   (2014) 15303–15316. doi:10.1021/ie4039532.

597 [33] E. Rodríguez, R. Palos, A. Gutiérrez, J.M. Arandes, J. Bilbao, Production of non-

598   conventional fuels by catalytic cracking of scrap tires pyrolysis oil, Ind. Eng.

599   Chem. Res. 58 (2019) 5158–5167. doi:10.1021/acs.iecr.9b00632.

600 [34] H. De Lasa, Riser Simulator, U.S. Patent, 5,102,628, 1992.

601 [35] E. Rodríguez, A. Gutiérrez, R. Palos, M.J. Azkoiti, J.M. Arandes, J. Bilbao,

602   Cracking of scrap tires pyrolysis oil in a fluidized bed reactor under catalytic

cracking unit conditions. Effects of operating conditions, Energy Fuels. 33 (2019) 3133–3143. doi:10.1021/acs.energyfuels.9b00292.

[36] E. Rodríguez, R. Palos, A. Gutiérrez, J.M. Arandes, J. Bilbao, Scrap tires pyrolysis oil as a co-feeding stream on the catalytic cracking of vacuum gasoil under fluid catalytic cracking conditions, Waste Manage. 105 (2020) 18–26. doi:10.1016/j.wasman.2020.01.026.

[37] E. Rodríguez, A. Gutiérrez, R. Palos, F.J. Vela, J.M. Arandes, J. Bilbao, Fuel production by cracking of polyolefins pyrolysis waxes under fluid catalytic cracking (FCC) operating conditions, Waste Manage. 93 (2019) 162–172. doi:10.1016/j.wasman.2019.05.005.

[38] S.S. Al-Khattaf, S.A. Ali, Catalytic cracking of arab super light crude oil to light olefins: An experimental and kinetic study, Energy Fuels. 32 (2018) 2334–2244. doi:10.1021/acs.energyfuels.7b04045.

[39] E. Rodríguez, A. Gutiérrez, R. Palos, F.J. Vela, M.J. Azkoiti, J.M. Arandes, J. Bilbao, Co-cracking of high-density polyethylene (HDPE) and vacuum gasoil (VGO) under refinery conditions, Chem. Eng. J. 382 (2020) 122602. doi:10.1016/j.cej.2019.122602.

[40] F.J. Passamonti, G. de la Puente, U. Sedran, Reconversion of olefinic cuts from fluidized catalytic cracking naphthas, Ind. Eng. Chem. Res. 43 (2004) 1405–1410. doi:10.1021/ie030467t.

[41] G. Wang, Z. Li, Y. Li, J. Gao, C. Xu, Y. Liang, X. Wang, Laboratory-scale experiments and industrial practice of low-temperature contact and high ratio of catalyst to oil in the FCC process, Energy Fuels. 27 (2013) 1555–1563. doi:10.1021/ef301690u.

627 [42] S. Abbasizadeh, S. Asadi, R. Karimzadeh, Kinetic modeling of LPG catalytic

628 cracking using Langmuir–Hinshelwood–Hougen–Watson theory, Res. Chem.

629 Intermed. 45 (2019) 5681–5703. doi:10.1007/s11164-019-03929-7.

630 [43] G. Uzcátegui, S.Y. Fong, A. de Klerk, Cracked naphtha reactivity: Effect of free

631 radical reactions, Energy Fuels. 32 (2018) 5812–5823.

632 doi:10.1021/acs.energyfuels.8b00656.

633 [44] R. Sadeghbeigi, Chemistry of FCC reactions, in: Fluid Catal. Crack. Handb., 2nd

634 ed., Gulf Professional Publishing, 2000: pp. 125–138. doi:10.1016/B978-

635 088415289-7/50005-6.

636 [45] A. Akah, M. Al-Ghrami, M. Saeed, M.A.B. Siddiqui, Reactivity of naphtha

637 fractions for light olefins production, Int. J. Ind. Chem. 8 (2017) 221–233.

638 doi:10.1007/s40090-016-0106-8.

639 [46] T.M. Moustafa, G.F. Froment, Kinetic modeling of coke formation and

640 deactivation in the catalytic cracking of vacuum gas oil, Ind. Eng. Chem. Res. 42

641 (2003) 14–25. doi:10.1021/ie0204538.

642 [47] A. Afshar Ebrahimi, H. Mousavi, H. Bayesteh, J. Towfighi, Nine-lumped kinetic

643 model for VGO catalytic cracking; using catalyst deactivation, Fuel. 231 (2018)

644 118–125. doi:10.1016/j.fuel.2018.04.126.

645 [48] H.S. Cerqueira, G. Caeiro, L. Costa, F. Ramôa Ribeiro, Deactivation of FCC

646 catalysts, J. Mol. Catal. A Chem. 292 (2008) 1–13.

647 doi:10.1016/j.molcata.2008.06.014.

648 [49] P. Wang, W. Zhang, H. Zhu, P. Yuan, C. Yang, C. Li, X. Bao, Insights into the

649 reaction pathway of n-butane conversion over HZSM-5 zeolite at low

650 temperature, Appl. Catal. A Gen. 584 (2019) 117135.

651   doi:10.1016/j.apcata.2019.117135.

652   [50]   H. Konno, T. Tago, Y. Nakasaka, R. Ohnaka, J.I. Nishimura, T. Masuda,

653   Effectiveness of nano-scale ZSM-5 zeolite and its deactivation mechanism on

654   catalytic cracking of representative hydrocarbons of naphtha, Microporous

655   Mesoporous Mater. 175 (2013) 25–33. doi:10.1016/j.micromeso.2013.03.016.

656   [51]   S.M. Alipour, Recent advances in naphtha catalytic cracking by nano ZSM-5: A

657   review, Chinese J. Catal. 37 (2016) 671–680. doi:10.1016/S1872-

658   2067(15)61091-9.

659   [52]   X. Zhang, D.G. Cheng, F. Chen, X. Zhan, n-Heptane catalytic cracking on

660   hierarchical ZSM-5 zeolite: The effect of mesopores, Chem. Eng. Sci. 168 (2017)

661   352–359. doi:10.1016/j.ces.2017.05.012.

662   [53]   E. Rodríguez, R. Palos, A. Gutiérrez, D. Trueba, J.M. Arandes, J. Bilbao,

663   Towards waste refinery: Co-feeding HDPE pyrolysis waxes with VGO into the

664   catalytic cracking unit, Energy Convers. Manage. 207 (2020) 112554.

665   doi:10.1016/j.enconman.2020.112554.

666   [54]   F.J. Passamonti, G. de la Puente, U. Sedran, Factors influencing the isobutane

667   yield during the conversion of vacuum gas oil (VGO) under fluidized catalytic

668   cracking (FCC) conditions, Ind. Eng. Chem. Res. 46 (2007) 9269–9273.

669   doi:10.1021/ie070880r.

670   [55]   M.A. den Hollander, M. Wissink, M. Makkee, J.A. Moulijn, Gasoline

671   conversion: reactivity towards cracking with equilibrated FCC and ZSM-5

672   catalysts, Appl. Catal. A Gen. 223 (2002) 85–102. doi:10.1016/S0926-

673   860X(01)00745-1.

674   [56]   R. Pujro, M. Falco, U. Sedran, Formation of aromatics in heavy gasoline and

675   light LCO ends in FCC, Appl. Catal. A Gen. 489 (2015) 123–130.

676   doi:10.1016/j.apcata.2014.09.051.

677 [57] M. Al-Sabawi, H. De Lasa, Modeling thermal and catalytic conversion of decalin

678   under industrial FCC operating conditions, Chem. Eng. Sci. 65 (2010) 626–644.

679   doi:10.1016/j.ces.2009.08.035.

680 [58] P.C. Anderson, J.M. Sharkey, R.P. Walsh, Calculation of the research octane

681   number of motor gasolines from gas chromatographic data and a new approach to

682   motor gasoline quality control, J. Inst. Pet. 58 (1972) 83–94.

683 [59] A.A. Al-Shammari, S.A. Ali, N. Al-Yassir, A.M. Aitani, K.E. Ogunronbi, K.A.

684   Al-Majnouni, S.S. Al-Khattaf, Catalytic cracking of heavy naphtha-range

685   hydrocarbons over different zeolites structures, Fuel Process. Technol. 122

686   (2014) 12–22. doi:10.1016/j.fuproc.2014.01.021.

687 [60] U.J. Etim, P. Bai, X. Liu, F. Subhan, R. Ullah, Z. Yan, Vanadium and nickel

688   deposition on FCC catalyst: Influence of residual catalyst acidity on catalytic

689   products, Microporous Mesoporous Mater. 273 (2019) 276–285.

690   doi:10.1016/j.micromeso.2018.07.011.

691 [61] D. Wallenstein, K. Schäfer, R.H. Harding, Impact of rare earth concentration and

692   matrix modification in FCC catalysts on their catalytic performance in a wide

693   array of operational parameters, Appl. Catal. A Gen. 502 (2015) 27–41.

694   doi:10.1016/j.apcata.2015.05.010.

695 [62] F.J. Passamonti, G. de la Puente, U. Sedran, Laboratory evaluation of FCC

696   commercial catalysts. Analysis of products of industrial importance, Catal.

697   Today. 133–135 (2008) 314–318. doi:10.1016/j.cattod.2007.12.123.